

# Visualization of hemiknot DNA structure with an atomic force microscope

Yuri L. Lyubchenko<sup>1,2,\*</sup>, Luda S. Shlyakhtenko<sup>2</sup>, Melinda Binus<sup>2</sup>, Claire Gaillard<sup>3</sup> and François Strauss<sup>3</sup>

<sup>1</sup>Department of Biology and <sup>2</sup>Department of Microbiology, Arizona State University, Tempe, AZ 85287-2701, USA and <sup>3</sup>Institut Jacques Monod, 2 Place Jussieu, 75251 Paris 05, France

Received July 19, 2002; Revised and Accepted September 24, 2002

## ABSTRACT

The hemiknot, a novel type of DNA structure in which a loop is stabilized by threading one end of the duplex through another, has been studied in this paper. The hemiknot was obtained by reassociation of a DNA fragment with (CA/TG)<sub>n</sub> inserts of different lengths. Slow and fast migrating products were purified by gel electrophoresis and imaged by atomic force microscopy (AFM) using the amino-propylsilatrane–mica technique for sample preparation. Slow migrating product was characterized by the formation of small blobs for the short insert (60 bp) and clear loops and other morphologies for the long insert (188 bp). These structural features were found in almost 100% of the molecules of the slow migrating sample and were not present in the control sample. Measurements showed that the location of the blobs coincided with the positions of the inserts. The sample with the 188 bp insert in the 573 bp fragment had large structural irregularities. The majority of the molecules (77%) had asymmetrically located loops. The location of the loop in the molecules correlated well with the position of the insert in the fragment. The measured sizes of the loops were in agreement with the insert size. Altogether, these data support the hypothesis for hemiknot formation suggested earlier. In addition to looped structures, other morphologies of the hemiknot were identified in AFM images. Possible models for hemiknot formation and structure are discussed.

## INTRODUCTION

Knots and catenanes are intermediates of DNA replication and recombination that should be removed for successful completion of these processes (1). Therefore, study of the formation of knots and catenanes *in vitro* will provide invaluable insight into understanding the mechanisms for removal of these topological DNA forms in the cell. Recently, the intracellular

formation of another joint topological intermediate, the hemicatenane, was observed (2). In this structure, two DNA strands are interlocked through the invasion of one strand of one duplex between the strands of another duplex. This structure is formed with a high yield in *Xenopus* extracts deficient in the replication machinery or that have had replication blocked with aphidicolin. The formation of hemicatenanes does not require DNA homology, but the search for homology between two duplexes can be facilitated if hemicatenanes are formed. Structural characterization of hemicatenanes will provide a background for understanding their biological effects. Our recent studies (3) found that reassociation of DNA fragments containing relatively large CA/TG repeats may lead to an intramolecular hemicatenane, in which the repeat forms a loop with two linear arms interconnected by the invasion of one single strand into the duplex. The schematic in Figure 1A illustrates how this novel structure is formed during the annealing of two complementary strands with CA/TG repeats. The formation of a slipped CA/TG duplex is a critical step for the conversion of the interlocked intermediate to the stable hemiknot structure. We will call this DNA structure a hemiknot in order to distinguish it from knots formed by DNA duplexes that do not involve threading one duplex into another (4). An attractive feature of the hemiknot is that this DNA structure can serve as a convenient model system for studies of the structure and dynamics of a hemicatenane.

The goals of this paper were, first, to provide direct evidence for hemiknot formation using AFM as a visualization tool and, second, to obtain structural characteristics of this novel, alternative DNA structure.

## MATERIALS AND METHODS

### Hemiknot DNA preparation

A 441 bp DNA fragment containing a 62 bp tract of poly(CA)·poly(TG) flanked by non-repetitive plasmid sequences (140 bp on one side and 239 bp on the other side) was obtained by digestion of plasmid pCG40 with *ScaI* and preparative electrophoresis. A 573 bp fragment containing a 188 bp CA/TG insert flanked by non-repetitive plasmid sequences (169 bp plus a 2 base overhang on one side, 214 bp plus a 2 base overhang on the other side) was obtained by

\*To whom correspondence should be addressed at Department of Microbiology, Arizona State University, PO Box 872701, Tempe, AZ 85287-2701, USA. Tel: +1 480 965 8430; Fax: +1 480 965 0098; Email: yuri.lyubchenko@asu.edu

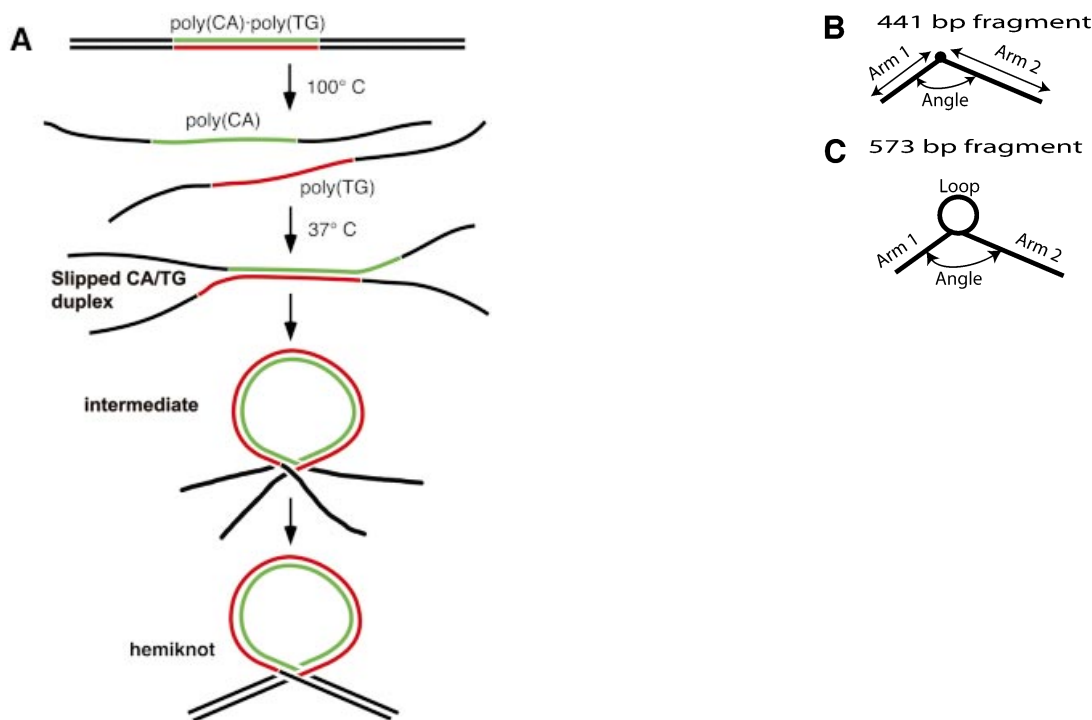


**Figure 1.** (A) The scheme of the DNA hemiknot structure formation. The novel structure is formed during annealing of two complementary strands with CA/TG repeats. The formation of a slipped CA/TG duplex is a critical step for the conversion of the interlocked looped intermediate to the stable hemiknot structure. (B and C) Schemes illustrating how the parameters for the 441 (B) and 573 bp (C) designs were measured.

digestion of plasmid pCA4 (GenBank accession no. AJ438270) with *Hin*PII and preparative electrophoresis.

Protein HMGB1 (formerly named HMG1) (5) was extracted from nuclei of cultured monkey kidney cells (CV-1 line) and purified by chromatography as described (6).

Hemiknot DNA with the short repeat was obtained by reassociation of the strands of the poly(CA)-poly(TG)-containing fragment in the presence of protein HMGB1 and was purified from linear DNA by preparative electrophoresis (7). The DNA fragment (~1 µg) in 25 µl of 10 mM Tris-HCl, 1 mM EDTA, pH 7.5, was denatured for 3 min at 100°C, transferred as quickly as possible to a tube containing ~20–50 ng HMGB1 in 75 µl of reassociation buffer (final composition for reassociation was 50 mM NaCl, 25 mM Tris-HCl, 1 mM DTT, 1 mM EDTA) and allowed to re-anneal for 30 min at 37°C. The sample was then extracted with chloroform/isoamyl alcohol in the presence of 1 M NaCl and 1% SDS, ethanol precipitated using linear polyacrylamide as carrier (8), redissolved and loaded on a 4% polyacrylamide gel (acrylamide:bis-acrylamide 29:1) in 6.7 mM Tris, 3.3 mM sodium acetate, 1 mM EDTA, pH 7.8, at 4°C with buffer recirculation. A similar sample prepared as a <sup>32</sup>P-end-labeled fragment was run in the adjacent lane as a position marker. Typical yield of the slow migrating sample (hemiknot DNA) was 10–15% of the total reaction products. In the absence of HMGB1 the efficiency of hemiknot DNA formation was small, ~1% (compare 3,7). Hemiknot DNA was cut from the gel, electroeluted onto a 1 M NaCl salt cushion and used for AFM imaging either directly or after ethanol precipitation and redissolution in 10 mM Tris-HCl pH 7.5, 1 mM EDTA, 100 mM NaCl.

The procedure for the preparation of the hemiknot DNA with a long repeat was similar except for the following modifications: with this fragment HMG was not used; the yield was extremely sensitive to the temperature of reassociation and to the concentration of the fragment, the best results (70% of slow migrating fractions) being obtained at 45°C and 0.1 µg/ml.

#### AFM procedures

Aminopropylsilatrane (APS)-mica was obtained by the treatment of freshly cleaved mica (Asheville-Schoemaker Mica Co., Newport News, VA) in a 0.17 mM solution of APS as described earlier (9). The AFM imaging procedure has been described elsewhere (10). Briefly, DNA samples (3–5 µl) were placed on APS-mica for 2 min, then the mica was rinsed with deionized water (Continental Water System Co., San Antonio, TX), after which the specimens were dried in an argon flow. Images were acquired by a MM SPM NanoScope IIIa system (Veeco/Digital Instruments, Santa Barbara, CA) operating in tapping mode in air at ambient conditions using OTESPA probes (Digital Instruments Inc.).

The lengths of both arms were recorded, as well as the loop sizes (see Fig. 1B and C). The angle between the two arms was also recorded. The length measurements of the arms were made by tracing the molecule from the junction of the hemiknot structure to the end of the molecule. The loop was measured by tracing the circular structure, trying to stay in the middle of the width of the molecule. The angle was found by placing the vertex at the junction of the hemiknot, then the molecule was traced on both arms for ~20–25 nm (see Fig. 1B and C).

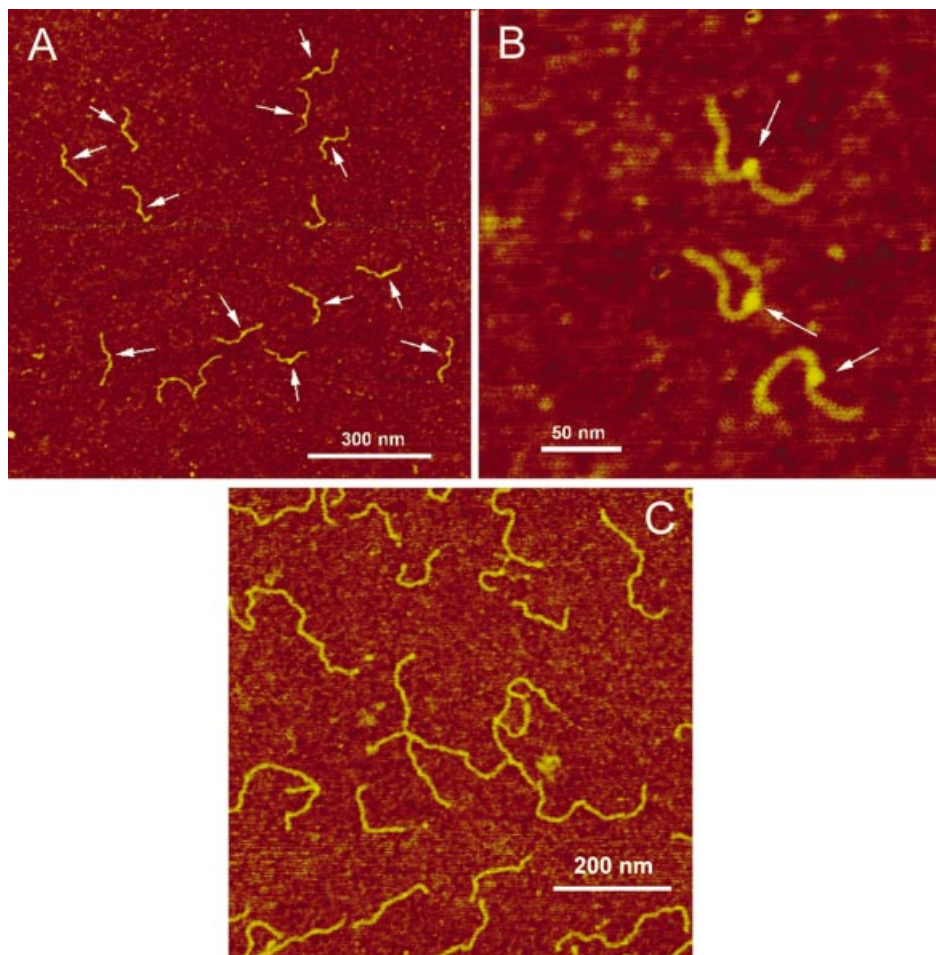


**Figure 2.** AFM images of the 447 bp fragment containing a hemiknot structure. (A and B) Large-scale image and a zoomed image with three clearly seen blobs, respectively. The blobs on the filaments are indicated with arrows. (C) AFM images of a control sample, an untreated 447 bp fragment. The samples were deposited onto APS-mica and imaged in air with TM AFM after the rinse-dry step.

## RESULTS

Two DNA fragments were designed for AFM studies of hemiknots. One fragment of 441 bp has the  $(CA/TG)_{31}$  insert located 140 bp from one of the ends. The second design has a 188 bp long  $(CA/TG)_{94}$  repeat located 172 bp from the closest end of the 573 bp long fragment.

### The structure of small hemiknot DNA

The hemiknot structures with the short repeat were obtained by the heating of linear fragments for 3 min at 100°C followed by annealing at 37°C for 30 min in the presence of HMGB1 protein. After deproteinization, the reaction mixture was separated on a polyacrylamide gel and the slowly migrating fraction of the sample (3,7) was eluted from the gel by electrophoresis and analyzed with AFM as described below.

**AFM images.** A large-scale AFM image of slow migrating molecules is shown in Figure 2A and a smaller scale image is shown in Figure 2B. The common feature of all the molecules is the presence of clear bright blobs indicated in the images with arrows. Some of the molecules have a clear kink at the

blob location. Such features are not found in the control sample (Fig. 2C). In each molecule the blob is located closer to one of the ends of the molecule and this finding is in qualitative agreement with the position of the insert in the molecule. We assume that the blob-like features we observed are small loops formed by DNA knotting. The following set of measurements supports this assumption.

**The location of blobs.** The positions of blobs on DNA molecules were determined by measuring the length of the short arm. The length measurements data are plotted as a histogram in Figure 3A. The distribution is very narrow and the mean distance is  $147 \pm 26$  bp. This number is very close to the distance from the repeat to the closest end of the fragment (140 bp).

**The size of the loop.** The histogram on the right in Figure 3A is the contour length of looped DNA filaments. The distribution is also rather narrow. The mean number for the contour length of the fragments is  $413 \pm 32$  bp. This number is less than the size of the original fragment,  $452 \pm 26$  bp (Fig. 3B). Assuming that the difference is due to the loop formation, we obtain a value of 39 bp for the loop size, which is less than the

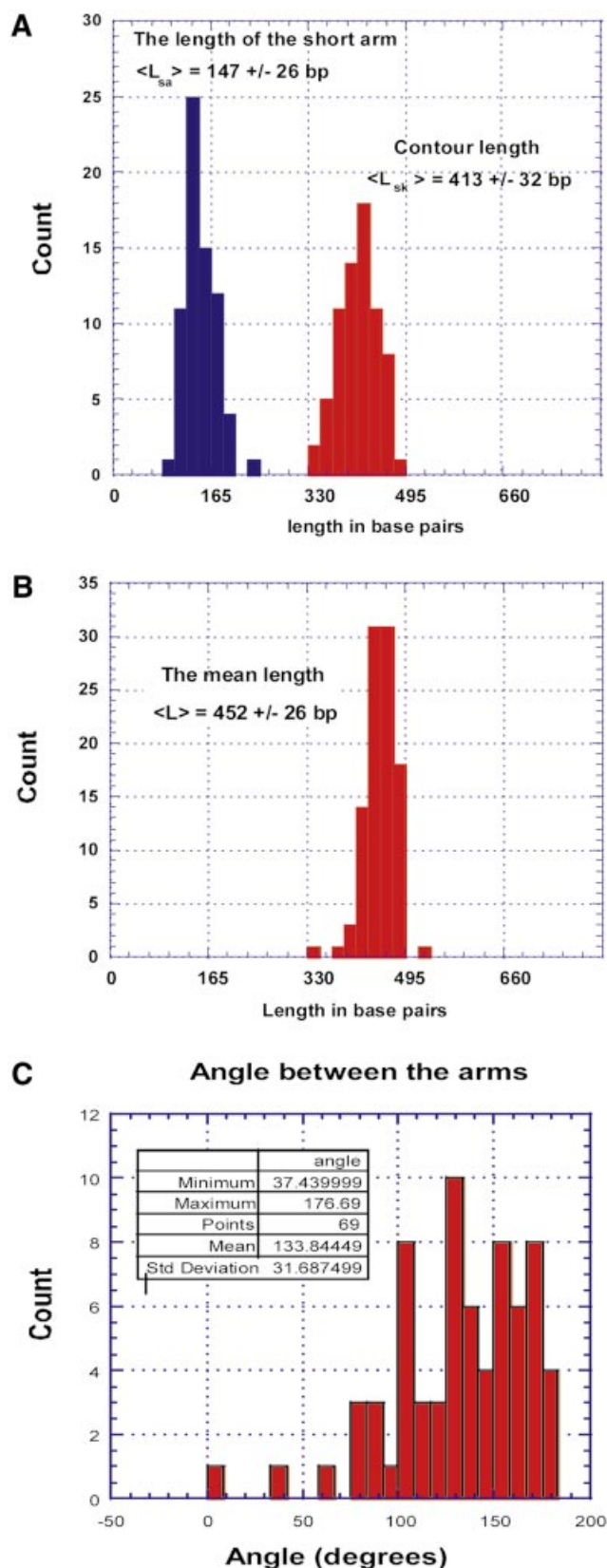


**Figure 3.** Data analysis for the 447 bp hemiknot. (A) The histograms for the short end-to-blob contour length distance (the length of the short arm) and the contour length for the entire hemiknot DNA molecule. (B) The contour lengths of the control 447 bp fragment. (C) The distribution of the inter-arm angle (the kink angle) around the blob.

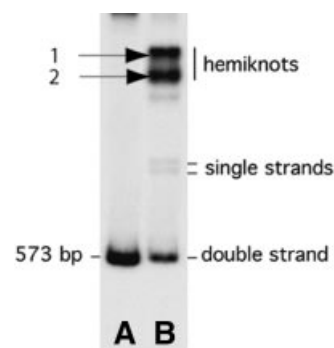


**Figure 4.** Gel electrophoresis of the hemiknot sample (lane B) obtained by annealing of the initially denatured 573 bp fragment containing the 188 bp CA/TG repeat. Positions of all the products are indicated. The control untreated fragment is shown in lane A.

60 bp length of the CA/TG repeat. The possible explanation of this small difference is given in the Discussion.

*The kink angle at the knot vicinity.* We measured the angle between the strands around the knot to characterize the hemiknot geometry. The histogram for this parameter is shown in Figure 3C. The mean number is rather large,  $135.2 \pm 29.4^\circ$ , indicating that the angle between the arms is very obtuse. The distribution is quite broad and there is a substantial population of molecules with almost no visible kink around the blob (the angle between the arms is  $\geq 150^\circ$ ).

#### The structure of the large hemiknot DNA

In order to visualize the loops directly and hence to obtain a detailed characterization of the hemiknot structure, a long CA/TG repeat was cloned into the plasmid. The hemiknot DNA with the large insert was prepared by annealing of the thermally denatured 573 bp fragment containing the 188 bp insert. The annealing reaction mixture was run in the gel and all the fractions were extracted from the gel. One such preparative gel is shown in Figure 4. Two thick slow migrating bands (1 and 2), presumably hemiknot DNA, are clearly seen in the gel. The yield of the slow migrating products was 10–20 times higher than the yield for the fragment with the short insert. Note that no HMG-type protein was used in the late stage of the annealing. The hemiknot samples were extracted from the gel, and the sample purified from the top band (no. 1) was used for AFM imaging.

*Imaging of the hemiknot structure and the loop position.* A large-scale image of the slow migrating sample is shown in Figure 5A. The molecules on the AFM images have clearly resolved irregularities typically seen as loops or large blobs. These features, indicated in the image with arrows, are located approximately in the middle of the molecules. A gallery of the small-scale images of the hemiknots with various morphologies is shown in Figure 5C and D. We arranged these images into three different categories. One of them with clearly identified loops (Fig. 5B) is the most representative class of the molecules (77%). Figure 5C illustrates the image of the hemiknots with a tight loop and Figure 5D shows the formation of structures with two loops. Each molecule was traced in order to illustrate the possible structure of the hemiknot.

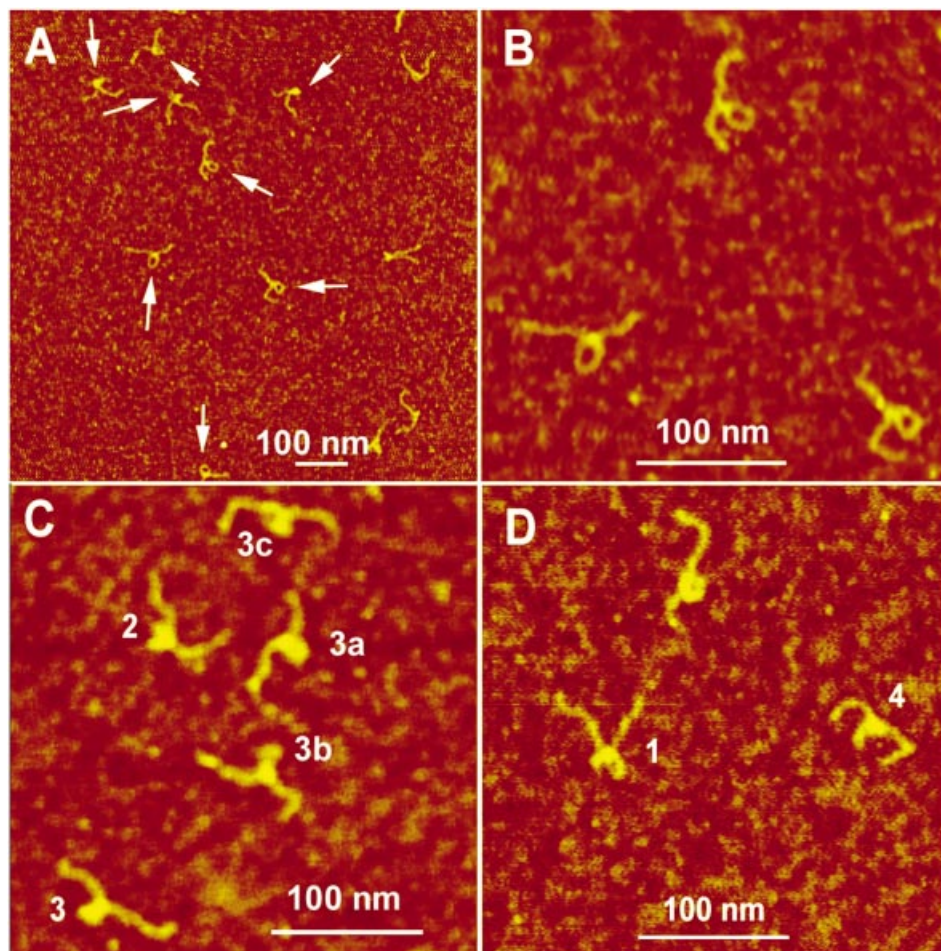


**Figure 5.** AFM images of the slow migrating (hemiknot) sample. (A) A large-scale image. Loops and other types of hemiknot structures are indicated with arrows. A series of high resolution images of different hemiknot morphologies is shown in (B)–(D), respectively. All images were taken in air by TM AFM.

*The parameters of the hemiknot structure.* The following parameters were measured: the lengths of each arm and the loop and the angle between the arms at the loop vicinity. The histograms in Figure 6A–C show the length distribution data for all parts of the looped molecules. Because the geometry of the DNA region within the loop may be different from B-helix geometry, the data are shown in nanometers. The values for these parameters are shown in Table 1 along with ratios of the arm 1 to arm 2 lengths and the loop to arm 2 lengths. The data are compared with the values calculated from the sequence data for the length of the insert and its position in the fragment. The arms ratio was  $0.74 \pm 0.18$  and this number is very close to the ratio calculated from the sequence, 0.79. Interestingly, the ratio between the sizes of the loop and arm 2 ( $0.54 \pm 0.12$ ) is also close to the expected value (0.49), suggesting that average linear DNA density within the loop is close to that for the B-helix geometry. The histogram for the angle between the arms for the sample with clearly identified loops (as shown in Fig. 5B) is shown in Figure 6D. The mean number for the inter-arm angle is  $123 \pm 32.2^\circ$ . It is slightly lower than the angle calculated for the hemiknot structures with the small insert (compare Fig. 3C).

## DISCUSSION

The AFM studies showed that the annealing of DNA fragments with CA/TG repeats leads to the formation of irregularities in the DNA filaments detectable by AFM. In the DNA fragment with the 60 bp CA/TG insert, the irregularities were imaged as thick blobs, whereas the structures of the irregularities can be resolved for the sample with the 188 bp CA/TG insert. In both DNA samples, the location of the irregularities and their sizes correlate with the positions and the sizes of the corresponding repeats, suggesting that these inserts are responsible for the formation of the structures observed with AFM.

Based on the AFM observations, we suggest the following mechanism for hemiknot structure formation (Figs 1A and 7) (see also 3). The reassociation proceeds through the formation of nucleation sites followed by formation of the entire duplex by zipping from the nucleation site. In the case where in-register pairing takes place, the duplex is formed through zipping in both directions. If nucleation happens inside the repeat, the pairing need not be in-register for the entire molecule because of the possibility of the  $(TG)_n$  strand sliding

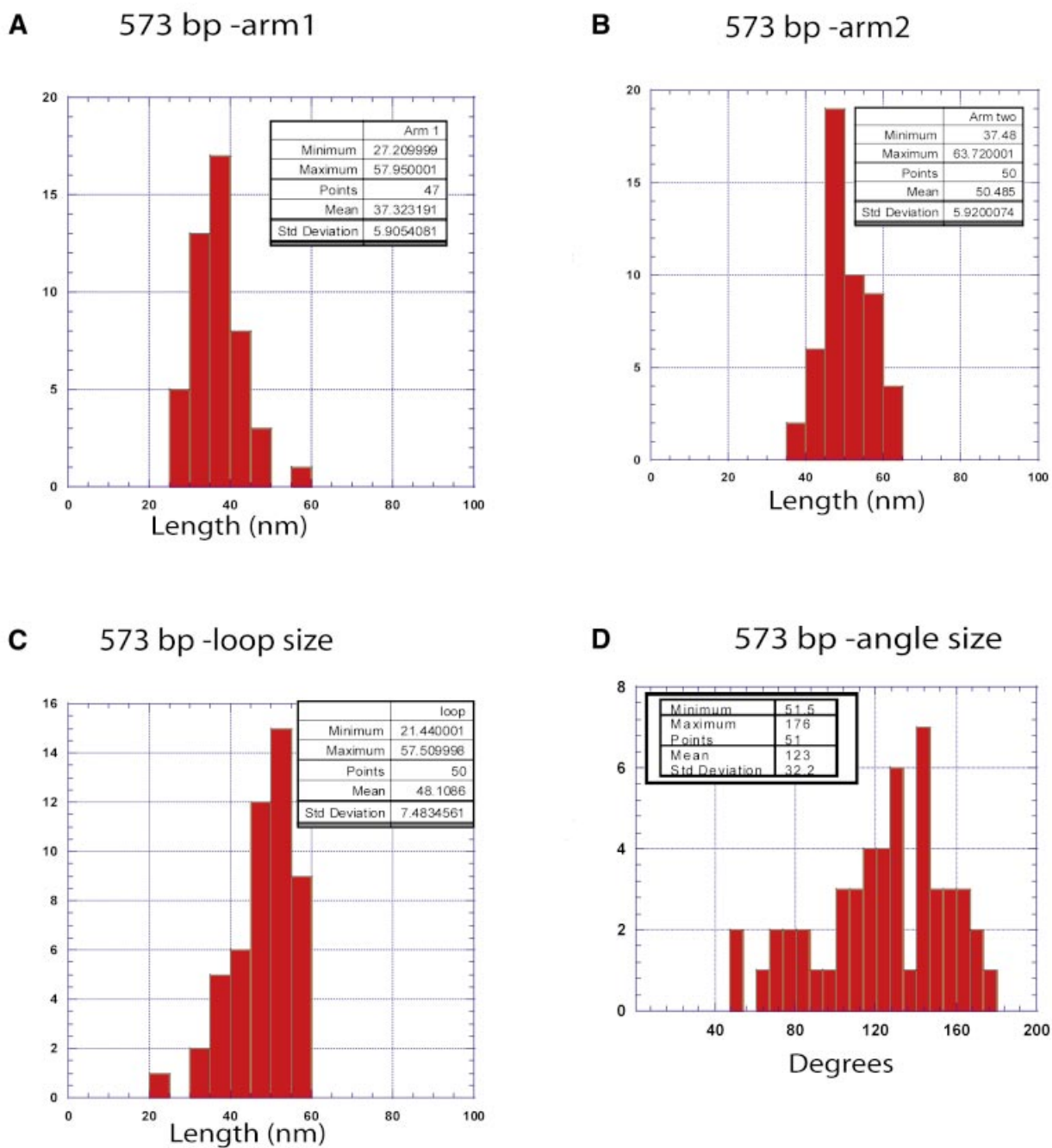


**Figure 6.** The histograms for the contour lengths of linear arms 1 (**A**) and 2 (**B**) and the loops (**C**) of the loop-type hemiknot (see Fig. 5B). (**D**) The distribution for the inter-arm angle. The statistics are shown in the boxes in the figure.

**Table 1.** The parameters of the hemiknot DNA structures with large loops

	Arm 1	Arm 2	Loop size	Arm 1:arm 2 ratio	Loop:arms ratio
Experimental values	37.3 ± 5.7 nm	50.5 ± 8.1 nm	48.1 ± 7.5 nm	0.74 ± 0.18	0.54 ± 0.12
Expected from the sequence	170 bp 44.4 nm <sup>a</sup>	215 bp 56 nm <sup>a</sup>	188 bp 49.1 nm <sup>a</sup>	0.79	0.49

<sup>a</sup>The conversion factor from base pairs to nanometers (0.26) was calculated from the AFM length measurements of a linear 573 bp fragment.

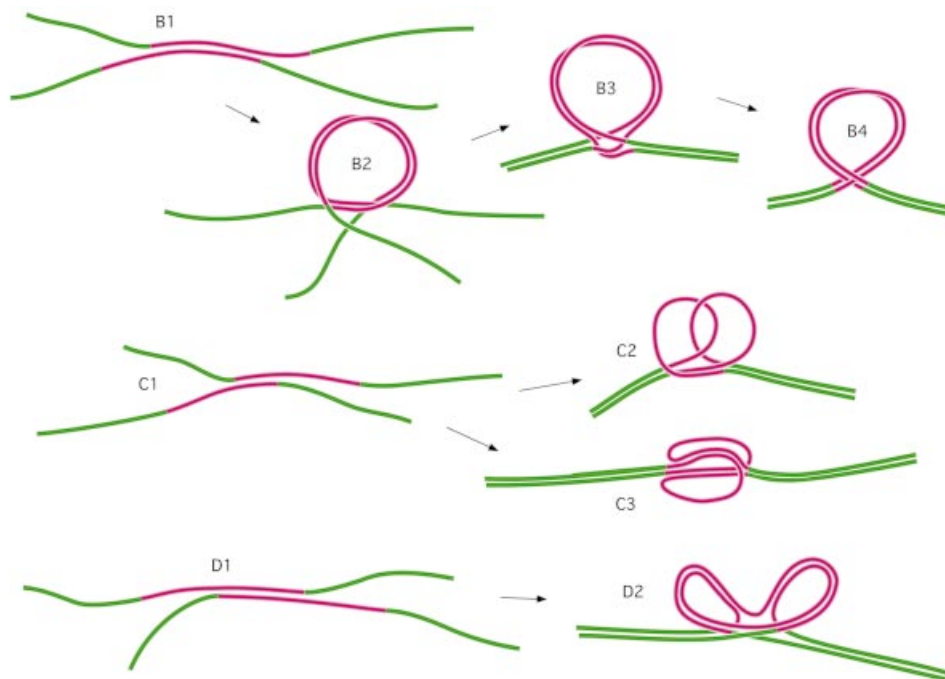


**Figure 7.** The scheme explaining the mechanism of hemiknot formation during reassociation of the fragment with the CA/TG repeat (pink). Path B illustrates formation of the hemiknot formed after reassociation within the repeat with a small misalignment. Paths C and D illustrate the formation of complex structures after the formation of a short helical region within the repeat with substantial misalignment of the strands.

along the  $(CA)_n$  strand. However, all other nucleation events within the repeat form intermediates that do not allow duplex formation through the fast zipping process (Fig. 7, paths B and C). An out-of-register nucleation requires sliding of the entire nucleated duplex until the in-register position is achieved. The formation of such a kinetically trapped state leads to a delay in the reassociation process allowing for the formation of intermediates of different kinds. For example, due to the high flexibility of single-stranded DNA (the persistence length is  $\sim 5$  nt) (11,12), relatively long unpaired ends adopt almost any possible configuration allowing the formation of structures like B2 with a large loop. The zipping of the rest of the molecule leads to the formation of a hemiknot structure with short unpaired regions (Fig. 7, B3) that can relax to a smoother circular region (B4). The formation of hemiknots with such structures is illustrated by the AFM images in Figure 5B. Short unpaired regions cannot be resolved in the images so the hemiknots look like perfect loops. However, these small loops can provide additional flexibility that explains the relatively broad distribution of the angle between the arms in Figures 3C and 6D.

However, nucleation can occur with a substantial shift (paths C and D in Fig. 7), so secondary nucleations and zipping of the rest of the molecule leads to the formation of hemiknots with large unpaired regions. The loops are complementary and can interact, but different structures can be formed due to the repetitive character of the sequence. Two model intermediates are shown in the scheme, and molecules in the images in Figure 5C and D confirm these models. Molecule 1 (Fig. 5D) clearly illustrates the loop interaction at the bottom (model C2); one of the unpaired regions is tightly folded, but we cannot exclude that this may have happened during deposition of the molecule onto the plane. We assume

that one of the arms in molecule 4 (Fig. 5D) points away from the surface and therefore it is visualized as a thick blob at the junction. Both regions in the two-loop intermediate can be folded, and molecule 2 in Figure 5C is one such example (compare scheme C3 in Fig. 7). Model D2, in which two loops interact, is illustrated by molecule 3. Molecules 3b and 3c are similar to molecule 3, although both unpaired regions in these molecules are too close to resolve them. The formation of such unpaired regions is explained by the stability of the hemiknot. Once formed, the hemiknot can migrate only via coordinated unwinding/overwinding fluctuations in the DNA segments within the loop and the rest of the molecule. Due to such pseudo-topological constraints, the base pairing within the hemiknot loop should lead to the formation of slowly dissipating negative supercoiling. We cannot exclude the possibility of the formation of left-handed helical regions because of the propensity of CA/TG repeats to adopt the Z-conformation (13), but we currently do not have direct experimental evidence for such a conformational transition within hemiknot DNA.

The model for the hemiknot assumes the looping out of repeated DNA regions and this process, similar to DNA cyclization, depends on the length of the loops. Indeed, the yield of the slow migrating fraction is very high ( $\sim 70\%$ , see Fig. 4). This high efficiency of hemiknot formation is consistent with DNA cyclization data (14,15) that show that DNA fragments of size 200–300 bp spontaneously form circles in ligase-mediated cyclization experiments. These results are explained by a relatively high DNA persistence length ( $\sim 150$  bp) (16). Therefore, DNA flexibility allows for the formation of loops of the sizes observed in this design. However, these considerations rule out the formation of hemiknots for the 60 bp CA/TG insert. If the hemiknot

structure corresponds to the thermodynamically stable configuration of a loop of this size, one can suggest that the DNA region inside the loop has a persistence length  $<40$  bp. There is evidence for increased flexibility of CA/TG repeats. Cyclization (17,18) and NMR studies (19) showed that CA tracts have elevated flexibility facilitating the formation of circles as small as 160 bp in ligation–cyclization experiments on a 21 bp repeat having an internal CA element. These conclusions are in line with crystallographic data (13) indicating conformational variability within CA tracts. Therefore, a tandem repeat of the CA motif can increase the flexibility of the entire (CA/TG)<sub>31</sub> insert, facilitating the formation of knots, but it is very unlikely that it will be sufficient to form stable circles as small as 60 bp. The presence of HMGB1 during the reassociation is a second factor explaining the possibility of forming small loops. HMGB1 is known to facilitate the cyclization of very small DNA fragments (20,21). The hemiknot forms with extremely low yield in a re-annealing reaction without the addition of proteins (22), whereas the yield of knots increased substantially in the presence of HMGB1 protein (7). The formation of very small loops in hemiknots is thus likely to be a synergistic effect of HMGB1 and the CA tracts.

Several lines of evidence indicate possible biological roles for the hemiknot or hemicatenane structure. Electron microscopy evidence revealed the formation of hemicatenanes as intermediates in DNA replication in SV40 (23). This observation is in line with the earlier results of Sundin and Varshavsky (4,24,25). Recently, Luccas and Hyrien (2) showed the formation of similar hemicatenanes by circular DNA molecules in *Xenopus* extracts when replication was blocked. Also of interest is the fact that the yield of small hemiknots increases dramatically in the presence of HMGB1 protein. HMG-type proteins are the most ubiquitous non-histone nuclear proteins in cells and their involvement in processes that require DNA strand separation may lead to hemiknot formation. Hemiknots may be formed in numerous genetic processes requiring the interaction of distantly separated regions via a DNA looping mechanism and by the transfer of the strand through the nick mediated by topoisomerase I.

## ACKNOWLEDGEMENTS

We thank S. Levene and R. Sinden for useful suggestions and C. McAllister for editing the manuscript. This research was supported by grants from the National Institute of Sciences (GM 62235), the National Science Foundation (DBI-0070356) and Digital Instruments/Veeco Inc. to Y.L.L.

## REFERENCES

- Vologodskii, A.V., Crisona, N.J., Laurie, B., Pieranski, P., Katritch, V., Dubochet, J. and Stasiak, A. (1998) Sedimentation and electrophoretic migration of DNA knots and catenanes. *J. Mol. Biol.*, **278**, 1–3.
- Lucas, I. and Hyrien, O. (2000) Hemicatenanes form upon inhibition of DNA replication. *Nucleic Acids Res.*, **28**, 2187–2193.
- Gaillard, C. and Strauss, F. (2000) DNA loops and semicatenated DNA junctions. *BMC Biochem.*, **1**, 1.
- Laurie, B., Katritch, V., Sogo, J., Koller, T., Dubochet, J. and Stasiak, A. (1998) Geometry and physics of catenanes applied to the study of DNA replication. *Biophys. J.*, **74**, 2815–2822.
- Bustin, M. (2001) Revised nomenclature for high mobility group (HMG) chromosomal proteins. *Trends Biochem. Sci.*, **26**, 152–153.
- Gaillard, C. and Strauss, F. (1994) Association of poly(CA)-poly(TG) DNA fragments into four-stranded complexes bound by HMG1 and 2. *Science*, **264**, 433–436.
- Gaillard, C. and Strauss, F. (2000) High affinity binding of proteins HMG1 and HMG2 to semicatenated DNA loops. *BMC Mol. Biol.*, **1**, 1.
- Gaillard, C. and Strauss, F. (1990) Ethanol precipitation of DNA with linear polyacrylamide as carrier. *Nucleic Acids Res.*, **18**, 378.
- Shlyakhtenko, L.S., Potaman, V.N., Sinden, R.R., Gall, A.A. and Lyubchenko, Y.L. (2000) Structure and dynamics of three-way DNA junctions: atomic force microscopy studies. *Nucleic Acids Res.*, **28**, 3472–3477.
- Shlyakhtenko, L.S., Potaman, V.N., Sinden, R.R. and Lyubchenko, Y.L. (1998) Structure and dynamics of supercoil-stabilized DNA cruciforms. *J. Mol. Biol.*, **280**, 61–72.
- Mills, J.B., Vacano, E. and Hagerman, P.J. (1999) Flexibility of single-stranded DNA: use of gapped duplex helices to determine the persistence lengths of poly(dT) and poly(dA). *J. Mol. Biol.*, **285**, 245–257.
- Rivetti, C., Walker, C. and Bustamante, C. (1998) Polymer chain statistics and conformational analysis of DNA molecules with bends or sections of different flexibility. *J. Mol. Biol.*, **280**, 41–59.
- Timsit, Y., Vilbois, E. and Moras, D. (1991) Base-pairing shift in the major groove of (CA)<sub>n</sub> tracts by B-DNA crystal structures. *Nature*, **354**, 167–170.
- Shore, D., Langowski, J. and Baldwin, R.L. (1981) DNA flexibility studied by covalent closure of short fragments into circles. *Proc. Natl Acad. Sci. USA*, **78**, 4833–4837.
- Shore, D. and Baldwin, R.L. (1983) Energetics of DNA twisting. I. Relation between twist and cyclization probability. *J. Mol. Biol.*, **170**, 957–981.
- Hagerman, P.J. (1988) Flexibility of DNA. *Annu. Rev. Biophys. Biophys. Chem.*, **17**, 265–286.
- Lyubchenko, Y., Shlyakhtenko, L., Chernov, B. and Harrington, R.E. (1991) DNA bending induced by Cro protein binding as demonstrated by gel electrophoresis. *Proc. Natl Acad. Sci. USA*, **88**, 5331–5334.
- Lyubchenko, Y.L., Shlyakhtenko, L.S., Appella, E. and Harrington, R.E. (1993) CA runs increase DNA flexibility in the complex of lambda Cro protein with the OR3 site. *Biochemistry*, **32**, 4121–4127.
- Russu, I.M. (1991) Studying DNA-protein interactions using NMR. *Trends Biotechnol.*, **9**, 96–104.
- Paull, T.T., Haykinson, M.J. and Johnson, R.C. (1993) The nonspecific DNA-binding and -bending proteins HMG1 and HMG2 promote the assembly of complex nucleoprotein structures. *Genes Dev.*, **7**, 1521–1534.
- Pil, P.M., Chow, C.S. and Lippard, S.J. (1993) High-mobility-group 1 protein mediates DNA bending as determined by ring closures. *Proc. Natl Acad. Sci. USA*, **90**, 9465–9469.
- Gaillard, C., Flavin, M., Woisard, A. and Strauss, F. (1999) Association of double-stranded DNA fragments into multistranded DNA structures. *Biopolymers*, **50**, 679–689.
- Sogo, J.M., Stahl, H., Koller, T. and Knippers, R. (1986) Structure of replicating simian virus 40 minichromosomes. The replication fork, core histone segregation and terminal structures. *J. Mol. Biol.*, **189**, 189–204.
- Sundin, O. and Varshavsky, A. (1980) Terminal stages of SV40 DNA replication proceed via multiply intertwined catenated dimers. *Cell*, **21**, 103–114.
- Sundin, O. and Varshavsky, A. (1981) Arrest of segregation leads to accumulation of highly intertwined catenated dimers: dissection of the final stages of SV40 DNA replication. *Cell*, **25**, 659–669.